



# A hybrid Kolmogorov-Arnold networks-based model with attention for predicting Arctic River streamflow

Renjie Zhou<sup>1,\*</sup>, Shiqi Liu<sup>2</sup>

5 <sup>1</sup>: Department of Environmental and Geosciences, Sam Houston State University, Huntsville, TX 77340, USA;  
Email: [renjie.zhou@shsu.edu](mailto:renjie.zhou@shsu.edu)

<sup>2</sup>: Key Laboratory of Water Cycle and Related Land Surface Processes, Institute of Geographic Sciences and Natural Resources Research, Chinese Academy of Sciences, Beijing, 100101, China; Email: [liusq@igsnr.ac.cn](mailto:liusq@igsnr.ac.cn)

*Correspondence to:* Renjie Zhou ([renjie.zhou@shsu.edu](mailto:renjie.zhou@shsu.edu))

10 **Abstract.** Arctic rivers represent important components of the Arctic and global hydrological and climate systems, serving as dynamic conduits between terrestrial and marine environments in some rapidly changing regions. They transport freshwater, sediments, nutrients, and carbon from vast watersheds to the Arctic Ocean and affect ocean circulation patterns and regional climate dynamics. Despite their importance, modeling Arctic rivers remains challenging because of sparse data networks, unique cryospheric dynamics, and complex responses to

15 hydrometeorological variables. In this study, a novel hybrid deep learning model is developed to address these challenges and predict Arctic River discharge by incorporating Kolmogorov-Arnold Networks (KAN), Long Short-Term Memory, and the attention mechanism with seasonal trigonometry encoding and physics-based constrains. It integrates several novel components: 1) The KAN-based deep learning component learns and captures intricate temporal patterns from nonlinear hydrometeorological data; 2) Explicit physical constrains designed for the

20 characteristics of permafrost-dominated watersheds govern snow accumulation and melt processes through the architectural design and loss function; 3) The seasonal variations are accounted for using trigonometry functions to represent cyclical patterns; 4) A residual compensation stricture allows the proposed model to revisit systematic errors in initial predictions and helps capture complex nonlinear processes that are not fully represented. The Kolyma River, which is significantly dominated by the permafrost, is adopted to test the performance of the newly

25 developed model. It obtains more robust and accurate predictive performance compared to baseline models. The role of physical constraints, the residual compensated architecture, and the trigonometry encoding are assessed by ablation analysis. The results indicate that these components positively contribute to improving the predictive performance. This novel approach addresses the unique challenges of hydrological forecasting in cold, permafrost-dominated regions and provides a robust framework for predicting Arctic River discharge under changing climate

30 conditions.

## 1. Introduction

Arctic rivers are integral to the Arctic's hydrological cycle and global climate systems and have undergone significant changes in recent years (Rawlins and Karmalkar, 2024). They are essential for transporting vast amounts



of freshwater, sediments, and organic matters from terrestrial sources to the Arctic Ocean and sustaining the  
35 biodiversity of the region and supporting unique ecosystems (Bring et al., 2016; Tank et al., 2023a; Vonk et al.,  
2025). The intricate connections between Arctic rivers and other cryospheric and atmospheric components make  
them highly sensitive to climate change (Feng et al., 2021). The response to climatic shifts, including changes in  
precipitation patterns, temperature regimes, snowmelt timing, and evapotranspiration rates in Arctic watersheds, has  
far-reaching implications for ecosystem stability and introduces significant uncertainties into future climate  
40 projections (Peterson et al., 2002).

Predicting hydrodynamics of Arctic rivers remains challenging due to the region's unique environmental conditions,  
data scarcity, complex feedback mechanisms, and their nonlinear responses to temperature, rainfall, and  
evapotranspiration. For example, warming temperatures can accelerate permafrost thaw and alter hydrological  
cycles in Arctic regimes. Temperature thresholds play a crucial role, particularly around the 0°C mark, where phase  
45 changes in precipitation and surface water create abrupt shifts in river dynamics (Prowse et al., 2011; Walvoord and  
Kurylyk, 2016). These temperature dependents transitions are further complicated by permafrost thawing, which  
destabilizes riverbanks, modifies groundwater flow paths, changes groundwater-surface water interactions, and  
increases sediment and nutrient loads, creating intricate feedback loops and complicates flow predictions  
(McClelland et al., 2004; Wang et al., 2021).

50 Over the last several decades, significant efforts have been directed towards forecasting the responses of river  
discharge to hydrometeorological conditions and understanding the underlying driving mechanisms (Gelfan et al.,  
2017; Jin et al., 2024a; Wang et al., 2021; Zhang et al., 2023; Zhou and Zhang, 2023a). These approaches can be  
broadly categorized into process-based models and empirical models. Process-based models simulate detailed  
physical and chemical processes within hydrological systems. For example, Gelfan et al. (2017) employed process-  
55 based hydrological models, including the HYdrological Predictions for the Environment (HYPE) and ECOlogical  
Model for Applied Geophysics (ECOMAG), to simulate the hydrodynamics of the Lena and Mackenzie Rivers and  
assessed the impacts of climate change. Similarly, Krogh et al. (2017) developed a physics-based hydrological  
model that accounted for key hydrological processes for quantifying water losses at the tundra-taiga transition in a  
small Arctic basin. While these process-based approaches yield valuable insights into the underlying hydrological  
60 processes and mechanisms, their successful implementation usually requires extensive parameterization and detailed  
characterization of environmental conditions, such as topography, spatially distributed hydrological parameters, and  
vegetation patterns. Such comprehensive data requirements pose significant challenges in Arctic regions, where  
remote locations, limited infrastructure, and harsh climatic conditions constrain field measurements and sustained  
monitoring campaigns (Gao et al., 2020). In contrast, empirical models, particularly data-driven approaches, focus  
65 on establishing direct mappings between input and output variables without requiring comprehensive understanding  
of the underlying hydrological systems (Zhou and Zhang, 2022b).

Recently, data driven models have been increasingly developed and used to simulate hydrodynamics and  
characterize hydrological systems in Arctic regions. For instance, Zhang et al. (2023) simulated the streamflow  
changes of several major Arctic rivers with meteorological conditions using a Support Vector Regression model.

70 This machine learning model was then used to estimate responses of these rivers to the elevated temperature and



precipitation conditions. Singh et al. (2020) implemented several convolutional neural networks models (CNN), including UNet, SegNet, Deeplab and DenseNet, to estimate surface concentration of river ice. Their approach demonstrated improved estimation performance compared to existing methods by addressing the key challenge of noise and errors in the limited available training data. Sergeev et al. (2024) developed a hybrid model integrating wavelet transform with long short-term memory (LSTM) networks for predicting Arctic methane concentration with greenhouse gases data monitored from the Belyy Island in Russia.

75

Despite these advances, significant challenges remain in modeling intricate river systems. Current deep learning approaches often struggle to capture complex and nonlinear relationships between meteorological variables and river discharge (Jin et al., 2024b; Zhou et al., 2024a). To improve the performance when dealing with nonlinear data such as rainfall-runoff relationship, many technologies have been developed. For example, Basu et al. (2022) proposed a nonlinear autoregressive model with exogenous variables for flooding prediction in Ireland. Bakhshi Ostadkalayeh et al. (2023) used Kalman Filter (KF) to manage nonlinear systems and improve LSTM performance for forecasting streamflow. Zhou et al. (2024b) integrated the ensemble empirical model decomposition technology with temporal fusion transformers and developed a new hybrid deep learning model for discharge prediction, which outperformed baseline models. Liu et al. (2024) proposed Kolmogorov-Arnold Networks (KAN) based on the theoretical foundation in the Kolmogorov-Arnold theorem. Unlike traditional neural networks that use fixed activation functions, the KAN model parameterized learnable activation functions on the connections between nodes, which significantly enhances the model's capacity to capture complex nonlinear relationships in data.

80

In addition, the scarcity of training data in Arctic regions limits the generalization of traditional deep learning models, leading to less satisfying performance (Alzubaidi et al., 2023). Physics-informed neural networks (PINN) and physics-guided deep learning approaches offer a promising solution by incorporating physical constraints and domain knowledge into the learning process (Karniadakis et al., 2021). By embedding physical laws into the loss function, these hybrid approaches can improve prediction accuracy while ensuring physically consistent results (Zhong et al., 2024). A variety of physics-informed deep learning models have been developed and demonstrated promising results in various hydrological applications. For example, Yang et al. (2020) proposed a hydrological model that integrated the physical process with a machine learning model for simulating daily streamflow. This hybrid model obtained accurate predictions for long-term daily streamflow with limited training data and demonstrated the effectiveness of this approach for reducing data requirements. Xie et al. (2021) integrated physical mechanisms into a deep learning model through both modified loss functions and synthetically generated training samples for forecasting streamflow. Their model outperformed traditional models and highlighted the value of incorporating physical constraints into deep learning frameworks for hydrological modeling.

85

90

95

100

To address these challenges and improve predictive performance in permafrost-dominated Arctic rivers, a novel hybrid residual compensated deep learning model that integrated seasonal patterns, physics-based constraints, KAN, LSTM and attention is proposed for forecasting Arctic River discharge in this study. This newly proposed model introduces several key innovations that serve specific purposes: (1) a KAN-based deep learning model coupled with LSTM and the attention mechanism, which enables sophisticated feature representation and temporal patterns recognition for nonlinear hydrometeorological data; (2) physical constrains that explicitly govern snow

105



accumulation and melt processes, which ensure physical consistency through the architectural design and loss function; (3) a residual compensation structure that combines a physics-informed main network with a specialized residual network, which allows the model to capture physically governed patterns and local anomalies; and (4) a temporal pattern recognition system that incorporates cyclical encoding of seasonal features for seasonal variations. This integrated approach is specifically designed to address the challenges of hydrological forecasting in cold, permafrost-dominated regions, where snow accumulation and melt play a crucial role in seasonal discharge patterns. The innovative components are integrated to enhance its predictive accuracy, physical consistency, and ability to handle complex seasonal dynamics and hydrological processes that characterize Arctic River systems.

## 2. Study area and data acquisition

To assess the performance, the newly developed model is tested on the Kolyma River located in the northeastern Siberia. The Kolyma River is one of the major Arctic rivers with a mean annual discharge of 136 km<sup>3</sup>/year and the largest river system draining into the East Siberian Sea. The Kolyma watershed is Earth's largest watershed that is 100% underlain by continuous permafrost (Holmes et al., 2012). The extensive permafrost coverage makes the Kolyma watershed particularly sensitive to climate warming, leading to its unique hydrological behaviors (Spencer et al., 2015). With a drainage basin of approximately 647,000 km<sup>2</sup>, the Kolyma River flows through diverse landscapes including the Kolyma Mountains, permafrost regions, and tundra ecosystems. The river's discharge regime is characterized by a distinctive seasonal pattern, with peak flows occurring during the spring snowmelt period (May-June) and low flows during the winter months when the river is ice-covered (Bring et al., 2016). In this study, monthly temperature ( $T$ ), precipitation ( $P$ ) and potential evapotranspiration ( $PET$ ) are used as input variables for forecasting discharge values of the Kolyma River. The Kolyma discharge records (1978-2020) at the Kolymsk gauge station (68.73°N, 158.72°E) are obtained from the ArcticGRO Discharge Dataset (Version 20231204). Note that the historical discharge data of the Kolyma River is not used as input variables in this study, which allows the model to establish direct relationships between hydrometeorological drivers and river discharge without incorporating autoregressive components, thereby focusing specifically on how climatic factors influence discharge patterns in permafrost-dominated watersheds. Gridded monthly average 2-m temperature and potential evapotranspiration with a resolution of 0.5° are obtained from CRU TS v. 4.07 (Harris et al., 2020). Additionally, monthly precipitation data at a 0.5° resolution are obtained from the Global Precipitation Climatology Centre (GPCC) dataset (Schneider et al., 2022). The complete dataset spans from January 1978 to December 2020, which is partitioned into training (80%) and testing (20%) datasets for model development and performance assessment.

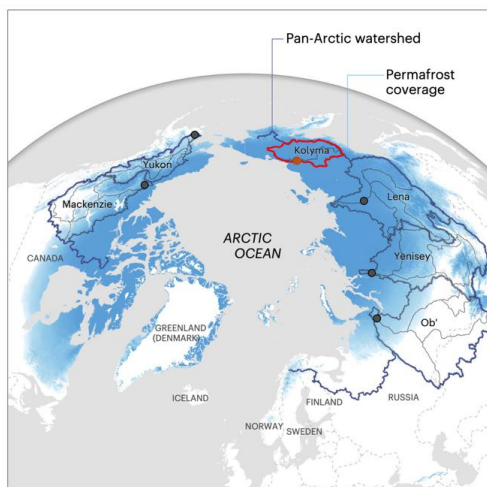


**Figure 1: The geographic location of the Kolyma River, modified from Tank et al. (2023b).**

### 3. Methodology

Hydrological forecasting in Arctic and permafrost-dominated regions presents unique challenges due to the strong influence of snow accumulation, permafrost thawing, and seasonal melt dynamics on river discharge. To address these issues, a novel hybrid residual-compensated physics-informed KAN-LSTM with attention model (RCPIKLA) that leverages strengths of multiple deep learning structures while embedding physical constraints related to snowmelt energy balance and seasonal variations directly into the training process for improved prediction accuracy and reliability.

As shown in Fig. 2, monthly precipitation, temperature and evapotranspiration data are preprocessed and standardized to ensure all features contribute appropriately to the training process. In regions dominated by permafrost, snow accumulation and melt typically exhibit strong seasonal periodicity (Andersson et al., 2021; Ernakovich et al., 2014). To include these cyclical patterns and facilitate smooth temporal transition, the month of the year is encoded using trigonometric transformations as  $\text{Month}_{\sin} = \sin\left(\frac{2\pi m}{12}\right)$  and  $\text{Month}_{\cos} = \cos\left(\frac{2\pi m}{12}\right)$ , where  $m$  refers to the month  $m \in \{1, 2, \dots, 12\}$ . The trigonometric features are concatenated with other input variables, including temperature, precipitation and evapotranspiration, and fed into the residual-compensated physics-informed KAN-LSTM model with attention. The newly proposed model leverages the KAN component as a feature transformation layer to extract and learn complex nonlinear patterns from hydrological and meteorological datasets. The LSTM component captures short- and long-term dependencies and effectively simulates sequential patterns and discharge variability. To further refine temporal learning, the attention mechanism is introduced and integrated, which allows the proposed model to selectively emphasize historically significant time steps, particularly those driving major and seasonal hydrological transitions. An important innovation is the residual compensation structure, which explicitly addresses the challenges of predicting extreme discharge events. By learning systematic



error patterns, the residual structure can adjust simulations based on residual predictions and improve performance during high-variability sceneries. Unlike conventional data-driven models that ignore fundamental physical constraints, the newly developed model incorporates physics-informed loss functions, ensuring that snow accumulation and melt timing adhere to thermodynamic energy balance principles. Additionally, the model employs seasonality-aware encoding using trigonometric transformations to recognize the cyclic nature of hydrological processes. This architecture is designed to provide an accurate and robust framework for forecasting river discharge in Arctic and permafrost-dominated environments.

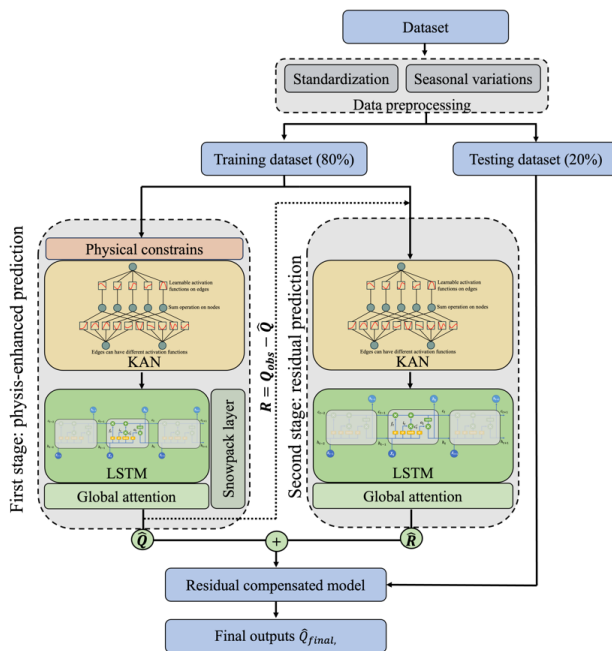


**Figure 2: The architecture of the residual compensated physics-informed KAN-LSTM model with attention.**

### 165 3.1. Kolmogorov-Arnold Networks

In the Kolmogorov-Arnold representation theorem, it states that any continuous multivariate function can be represented as a superposition of continuous functions of a single variable (Kůrková, 1992). Based on this theoretical foundation and the mechanism of decomposing the multivariate function into various univariate functions, the Kolmogorov-Arnold Networks model (KAN) was developed by replacing all weight parameters with univariate functions parameterized as splines, rather than using Multi-Layer Perceptrons (MLPs) in traditional neural networks (Liu et al., 2024). This structure allows the KAN model to dynamically adapt its processing to various aspects of the data and emphasize finer details by modulating the granularity of these splines (Granata et al., 2024). With learnable activation functions and structured transformations, it can effectively extract nonlinear



relationships and capture intricate patterns, making it well-suited for modeling complex hydrological systems like  
 175 Arctic River discharge.

In this newly developed hybrid model, the KAN module is used as an advanced feature transformation block and a  
 nonlinear feature extractor that processes raw hydrological and meteorological inputs before the sequential modeling  
 stage. The architecture of the KAN module is composed of several parts: 1) input expansion: the raw input features  
 including precipitation, temperature and evapotranspiration are first projected into a higher dimensional space by a  
 180 fully connected layer that increases the representational capacity. The dimension expansion of the input features  
 allows the model to isolate some nonlinear interactions between variables, such as temperature-driven snowmelt  
 thresholds or precipitation-phase transitions; 2) Nonlinear activation: a Gaussian Error Linear Unit (GELU)  
 activation is then applied to the expanded features. The GELU function introduces smooth nonlinearity and enables  
 the network to capture intricate patterns in the input data, which approximates the role of univariate functions in the  
 185 Kolmogorov-Arnold theorem while avoids the computational overhead of spline optimization; 3) Dimensionality  
 reduction: a second linear layer then compresses the activated features down to a lower-dimensional space which is  
 then fused with physics-based constrains, such as snowpack dynamics and fed into the LSTM-Attention network for  
 temporal integration. It aims at effectively distilling the information into a compact, yet expressive representation  
 that is more amenable for subsequent processing. The KAN transformation and processing steps can be expressed as  
 190 the following equations accordingly:

$$H_1 = W_1 X + b_1, \tag{1}$$

$$H_2 = GELU(H_1), \tag{2}$$

$$KAN(X) = W_2 H_2 + b_2, \tag{3}$$

where  $X$  is the input features;  $W_1$  and  $W_2$  refer to the expansion and compression weight matrices;  $b_1$  and  $b_2$  are the  
 195 corresponding bias vectors; GELU is the Gaussian Error Linear Unit activation function.

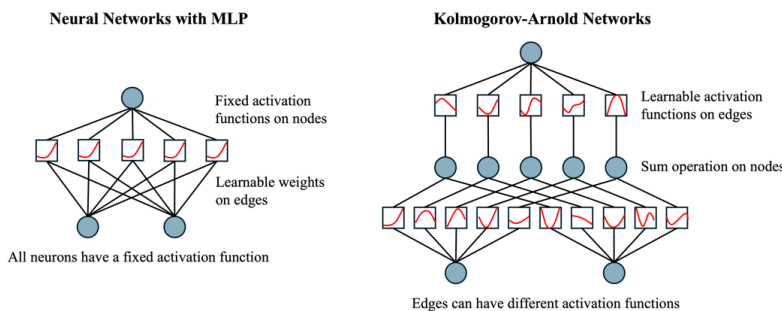


**Figure 3: The structure of Kolmogorov-Arnold Networks (KAN) compared to MLP.**

### 3.2. Long Short-Term Memory

Following the Kolmogorov-Arnold transformation, the processed input features will enter the Long Short-Term  
 Memory (LSTM) module. LSTM is a modified variant of recurrent neural networks (RNNs), specifically designed  
 to address the vanishing gradient problem while learning long-term dependencies in sequential data (Hochreiter and  
 200 Schmidhuber, 1997). By incorporating the gating mechanism and a hidden state, LSTM can efficiently regulate



information flow through the network and selectively remember or forget information in long sequences. Because of its ability to capture temporal dependencies inherent in river systems, the LSTM model has been widely used in a variety of hydrological models (Gao et al., 2020; Zhou and Zhang, 2023b). It aims at learning and identifying important historical patterns in meteorological variables (such as temperature and precipitation) that influence current river discharge, while simultaneously recognizing the varying time lags between these inputs and their hydrological responses. This capability makes LSTMs especially suitable for modeling Arctic River systems, where discharge patterns are influenced by both immediate meteorological conditions and longer-term processes such as snowmelt and permafrost dynamics (Kratzert et al., 2018).

The memory cell of LSTM is primarily composed of three gates: the input gate ( $i_t$ ), forget gate ( $f_t$ ), and output gate ( $o_t$ ). The input gate determines which new information should be stored in the cell state, while the forget gate decides what information should be discarded from the previous cell state. The output gate controls how much of the cell state should be exposed to the next layer. This gating mechanism allows LSTMs to maintain and update relevant information over long sequences while filtering out irrelevant details (Hochreiter and Schmidhuber, 1997). At any time step  $t$ , the hidden state ( $h_t$ ) and the cell state ( $c_t$ ) are calculated based on the previous hidden state ( $h_{t-1}$ ) and cell state ( $c_{t-1}$ ) with three logic gates as follows:

$$f_t = \sigma(W_f X_t + U_f h_{t-1} + b_f), \quad (4)$$

$$i_t = \sigma(W_i X_t + U_i h_{t-1} + b_i), \quad (5)$$

$$c'_t = \tanh(W_c X_t + U_c h_{t-1} + b_c), \quad (6)$$

$$c_t = f_t \otimes c_{t-1} + i_t \otimes c'_t, \quad (7)$$

$$o_t = \sigma(W_o X_t + U_o h_{t-1} + b_o), \quad (8)$$

$$h_t = o_t \otimes \tanh(c_t), \quad (9)$$

Where  $c_t$ ,  $c'_t$ , and  $h_t$  are the cell state, candidate cell state, and hidden state at time step  $t$ , respectively;  $X_t$  refers to the input variables processed by the KAN module;  $W$ ,  $U$  and  $b$  are weight matrices and bias vectors whereas subscripts  $f$ ,  $i$ ,  $c$ , and  $o$  denote the forget gate, input gate, candidate cell, and output gate;  $\sigma$  and  $\tanh$  are the sigmoid and hyperbolic tangent activation functions;  $\otimes$  is the element-wise operation.

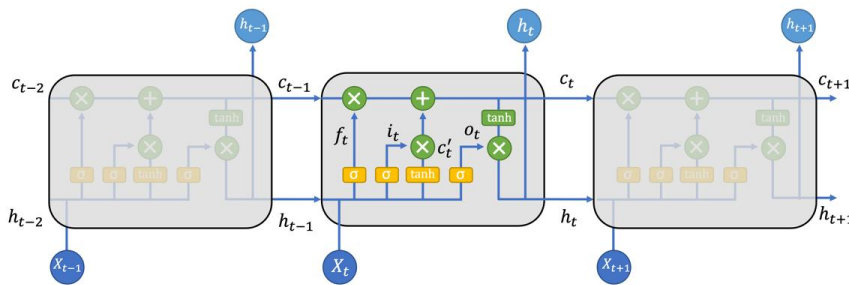


**Figure 4: The architecture of the LSTM model.**

### 3.3. Attention





A global attention mechanism is incorporated into the LSTM component of the newly proposed model to assign different importance weights to past time steps when making predictions, which enables the model to dynamically weight and aggregate information across temporal sequences. As the influence of historical conditions on current discharge exhibits complex temporal dependencies in hydrological modeling, the attention mechanism can help capture both short-term fluctuations and long-range interactions in input variables. The attention score for each time step can be computed as (Vaswani et al., 2017):

$$e_t = v^T \tanh(W_a h_t + b_a), \quad (10)$$

$$\alpha_t = \frac{\exp(e_t)}{\sum_j \exp(e_j)}, \quad (11)$$

$$C = \sum_t \alpha_t h_t, \quad (12)$$

$$\hat{Q} = W_c C + b_c, \quad (13)$$

where  $W$  and  $b$  denote weight and bias parameters;  $e_t$  refers to the attention score at time step  $t$ ;  $h_t$  is the hidden state from the LSTM component at time step  $t$ ;  $v$  is a learnable vector which determines the importance of each hidden state;  $\alpha_t$  is the attention weight;  $C$  is the context vector that represents a weighted sum of all hidden states;  $\hat{Q}$  refers the discharge prediction using the context vector calculated from the context vector.

### 3.4. Physics-informed mechanisms

Physics-informed neural networks improve hydrological modeling by combining established physical information with deep learning architectures, which creates a synergistic approach that leverages the strengths of both methodologies. In this study, a hybrid physics-informed approach is implemented through two complementary mechanisms: 1) a dedicated snowpack layer directly integrated into the model architecture, and 2) a physics-constrained loss function. The snowpack layer explicitly simulates snow accumulation and melting processes based on temperature and precipitation. It tracks precipitation falling as snow when temperatures drop below freezing ( $T < 0^\circ\text{C}$ , where  $T$  represents temperature) and computes snowmelt using a temperature-dependent rate function (Hock, 2003):

$$M_r = f_m \cdot \max(T, 0), \quad (14)$$

where  $M_r$  is the melting rate, and  $f_m$  is the melting factor coefficient. The melting factor of  $0.5 \text{ mm}/^\circ\text{C}/\text{day}$  is adopted in this study based on empirical studies of Arctic snowpack dynamics (Hock, 2003). The snowpack mass balance is estimated as follows (DeWalle and Rango, 2008):

$$S_t = S_{t-1} + P_t^{\text{snow}} - M_t, \quad (15)$$

where  $S_t$  and  $S_{t-1}$  denote the snowpack water equivalent at time  $t$  and  $t-1$ ;  $M_t$  is the actual snowmelt, which is calculated as  $M_t = \min(S_{t-1}, M_r)$ ;  $P_t^{\text{snow}}$  refers to the snowfall fraction of precipitation, which is determined by the following equation (Harpold et al., 2017):

$$P_t^{\text{snow}} = \begin{cases} P_t, & \text{if } T < 0^\circ\text{C} \\ 0, & \text{otherwise} \end{cases} \quad (16)$$

where  $P_t$  is the precipitation rate. A key architectural innovation is that the calculated snowmelt amount is directly added to the data-driven neural network output before the final activation function of the first stage as shown in Fig. 2, creating a hybrid prediction that leverages both physical understanding and learned patterns:



$$\hat{Q} = \text{ReLU}(Q_{LSTM} + M_t), \quad (17)$$

Where  $\hat{Q}_i$  and  $Q_{LSTM}$  are the predicted discharge from the first stage and the output from the LSTM with attention component, respectively; ReLU refers to rectified linear unit activation function.

265 In addition to the snowpack layer, a physics-constrained loss function is implemented for enforcing physical consistency through the term:

$$\mathcal{L}_{phys} = \frac{1}{n} \sum_i \max(M_t - \hat{Q}_i, 0), \quad (18)$$

where  $n$  is the number of samples, and  $\mathcal{L}_{phys}$  refers to the physics-constrained loss function term. This term penalizes physically inconsistent predictions where the modeled discharge is less than the calculated snowmelt contribution. This dual physics-guided approach is particularly valuable for Arctic rivers where seasonal snow accumulation and permafrost melt dominate the hydrological regime. In these regions, river discharge often exhibits complex, threshold-dependent behaviors and memory effects related to temperature-controlled phase changes in water, processes that purely statistical models often struggle to capture accurately without explicit physical constraints. By incorporating both a direct snowmelt contribution mechanism and physics-consistency loss penalties, 275 the proposed model maintains physical realism even when data limitations exist.

### 3.5. Residual compensated mechanism

While the physics-informed deep learning model may improve prediction accuracy by embedding domain knowledge, they may still fail to capture certain discrepancies between observed and predicted discharge values caused by sources, such model simplifications, missing hydrological processes, noise in the input data, and extreme 280 events. To address this limitation, a residual compensated mechanism is incorporated. As shown in Fig. 2, the residual compensated framework in the newly proposed model operates in a two-stage process. First, we train a physics-informed KAN-LSTM model that incorporates snowpack dynamics and constraints through the combined loss function ( $\mathcal{L}_{combined}$ ):

$$\mathcal{L}_{combined} = \alpha \mathcal{L}_{MSE}(\hat{Q}, Q_{obs}) + \beta \mathcal{L}_{phys}, \quad (19)$$

285 where  $\mathcal{L}_{MSE}$  refers to the mean squared error between the prediction  $\hat{Q}$  and the observation  $Q_{obs}$ ;  $\alpha$  and  $\beta$  are weighting coefficients which can be obtained by trial-and-error. In the second stage, the residuals ( $R_i$ ) between observations and physics-based predictions are computed:  $R_i = Q_{obs,i} - \hat{Q}_i$ . These residuals represent the information discrepancies that the physics-informed KAN-LSTM model fails to capture. A separate residual model ( $M_{res}$ ) which has a KAN-LSTM architecture without physics-informed components is trained to specifically learn 290 the discrepancies:  $\hat{R}_i = M_{res}(X_i)$ . The final discharge prediction ( $\hat{Q}_{final,i}$ ) is obtained by combining results from the first and second stage:

$$\hat{Q}_{final,i} = \hat{Q}_i + \hat{R}_i. \quad (20)$$

This residual compensated approach has several advantages: on one hand, it preserves the physical consistency by incorporating the physics-informed component during the first stage. On the other hand, the residual prediction in 295 the second stage can focus exclusively on missed patterns and systematic anomalies, creating a specialized representation for complex processes. As a result, it enables end-to-end training where each component focuses on



complementary aspects of the hydrological system: the physics-informed deep learning model captures the first-order processes driven by hydrometeorological variables, while the residual model captures secondary influences and complex feedback mechanisms. It is especially benefit for Arctic River systems, where seasonal transitions and complex cryospheric processes may not be fully captured by simplified physics representations.

### 3.6. Evaluation metrics

To assess the performance of the proposed model in the Kolyma River, two popular evaluation metrics are adopted in this study: Nash-Sutcliffe Efficiency (NSE) and Root Mean Square Error (RMSE) (An et al., 2020; Zhou and Zhang, 2022a). NSE is a dimensionless metric widely used in hydrological modeling that measures how well the model predictions match the observed data compared to using the mean of the observations as a predictor. An NSE value of 1 indicates a perfect fit, while values approaching zero or negative suggest that the model performs no better than using the mean value of the observed data. The NSE value can be calculated as:

$$NSE = 1 - \frac{\sum_{i=1}^n (Q_{obs,i} - \hat{Q}_{final,i})^2}{\sum_{i=1}^n (Q_{obs,i} - \bar{Q})^2}, \quad (21)$$

where  $Q_{obs,i}$  and  $\bar{Q}$  are the observed discharge value at time step  $t$  and the average discharge, respectively. In hydrological modeling, NSE values above 0.75 indicate very good model performance (D. N. Moriasi et al., 2007). RMSE is an absolute error metric that quantifies the average magnitude of prediction errors in the original units of discharge being predicted. RMSE gives higher weight to large errors due to its squared terms, which makes it particularly useful for evaluating models where large errors are especially undesirable, such as in flood prediction. Lower RMSE values indicate better model performance, with RMSE = 0 representing a perfect fit. It is defined as:

$$RMSE = \sqrt{\frac{1}{n} \sum_{i=1}^n (Q_{obs,i} - \hat{Q}_{final,i})^2}. \quad (22)$$

These two metrics complement each other in our evaluation framework. While NSE provides a normalized measure that facilitates comparison across different time periods, RMSE provides an intuitive measure of error magnitude in the original units. Together, they provide a comprehensive assessment of the model's ability to capture both the temporal dynamics through NSE and the absolute accuracy through RMSE of river discharge predictions in the Kolyma River system.

## 4. Results

### 4.1. Performance comparison among various baseline models with various time steps

The newly proposed model and baseline models are trained in the training dataset of the Kolyma River, and then the fine-tuned models are applied to the unseen testing dataset for the assessment of the predictive performance. The model performance across different time steps (1-12 months) reveals variations in predictive capabilities among the models tested. To ensure stable results, each model is run 10 times at each time step, and the evaluation metrics are averaged. Presented in Fig. 5, it shows the comparison of NSE values (Fig. 5 Left) and RMSE values (Fig. 5 Right) for the Kolyma River discharge predictions using several different model architectures, which include the simple RNN, LSTM, and GRU models, which are popular temporal baseline models widely used in many hydrological



330 studies, and the newly proposed Residual Compensated Physics-Informed KAN-LSTM with Attention (RCPIKLA).  
The NSE values demonstrate that the newly proposed RCPIKLA model consistently outperforms all baseline models  
across all time steps, achieving the highest NSE values ranging from 0.78 to 0.86. This superior performance is  
particularly obvious at the time step of 9 months, where RCPIKLA reaches peak NSE values of approximately 0.86.  
The traditional deep learning models, including the simple RNN, GRU, and LSTM models, show similar  
335 performance patterns with NSE values ranging between 0.65 and 0.76. These models exhibit a noticeable decline in  
performance at medium-range time steps (4-8 months), with their lowest NSE values observed around months 5-6,  
which suggests limitations in capturing seasonal transitions in Arctic River systems. The RMSE analysis  
corroborates these findings, with RCPIKLA achieving the lowest error values (6.5 mm -8.5 mm) across all time  
steps. Again, the RCPIKLA model demonstrates substantially lower prediction errors compared to other baseline  
340 approaches, which exhibit RMSE values ranging from 9.5 mm to 11.5 mm. The higher RMSE values for Simple  
RNN, GRU, and LSTM at medium-range time steps further highlight their difficulties in accurately predicting  
discharge during critical seasonal transition periods.

To further evaluate the robustness and generalization ability of each model, we conduct the box plots of 10  
independent runs for each architecture and compute the distributions of NSE and RMSE across all time steps. These  
345 box plots, as shown in Figure 7, provide insight into the statistical variability and stability of model performance.  
The RCPIKLA model demonstrates the best overall performance with the highest median NSE and lowest median  
RMSE, along with the narrowest interquartile range. This indicates not only high accuracy but also low variability  
across runs, suggesting a stable learning and prediction process. Moreover, outliers are less frequent and less  
extreme for RCPIKLA, which indicates a consistently reliable model output. LSTM and Simple RNN exhibit greater  
350 variance in both NSE and RMSE distributions, with wider interquartile ranges and more outliers. This means higher  
sensitivity to random initialization and potential overfitting or underfitting in different runs. GRU shows moderately  
better consistency than LSTM and Simple RNN but still falls short of the stability achieved by RCPIKLA. The  
newly proposed RCPIKLA model consistently outperforms all other models across different time steps and obtains  
robust performance. These results demonstrate that incorporating physical constraints with the KAN-LSTM model  
355 and complementing them with residual learning significantly improve predictive performance for capturing complex  
patterns in Arctic River discharge.

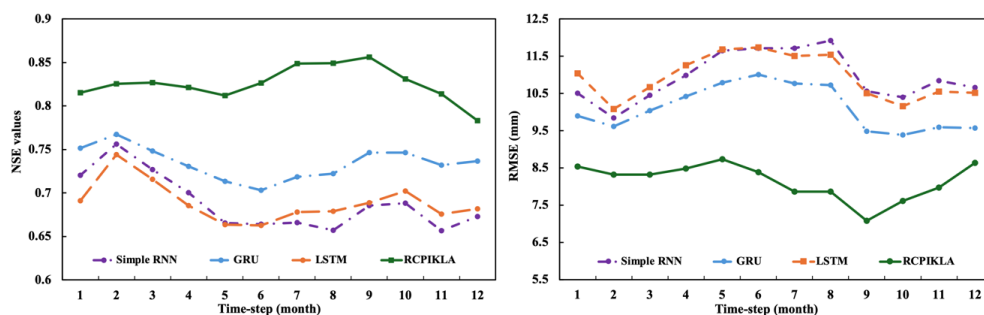




**Figure 5: NSE (left) and RMSE (right) values of multiple models over various time steps. The models include the residual-compensated physics-informed KAN-LSTM model with attention (RCPIKLA), simple RNN, LSTM, and GRU.**

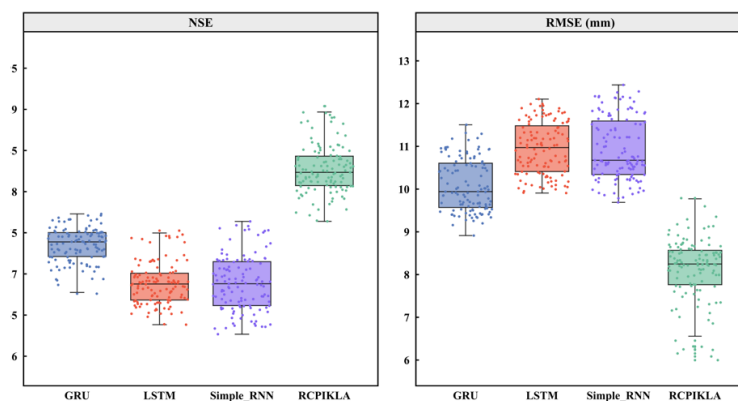


**Figure 6: The box plot of NSE (left) and RMSE (right) values of multiple models of various time steps (1-12 months) for 10 runs.**

#### 4.2. Performance comparison among various deep learning models at different value ranges

As shown in Fig. 5, the optimal performance of the proposed RCPIKLA model is obtained when the time step is 9 months. In addition to temporal comparisons, the predictive performance across different discharge value ranges is further assessed to understand how well each model captures the full spectrum of hydrological variability. The predicted and observed values of the proposed model and baselines when the time step is 9 months are presented in Fig. 7. The red dash line angled at 45 degrees represents the line of perfect agreement between observed and predicted values. The performance metrics reveal substantial differences in model accuracy. The RCPIKLA model demonstrates more robust performance compared to others across all value ranges with the highest NSE coefficient of 0.856 and the lowest RMSE of 7.077 mm. This indicates that the proposed hybrid approach, which integrates physics-informed constraints with residual compensation, captures the nonlinear and non-stationary characteristics of the Kolyma River discharge more effectively than other architectures. The GRU model achieves an intermediate performance level (NSE = 0.750, RMSE = 9.418 mm), which overperforms other recurrent neural networks but falling short of KNN based models. Both LSTM and Simple RNN exhibit similar and relatively poorer performance metrics, which demonstrates their limitations in capturing the complex hydrological dynamics of Arctic River systems when used without additional enhancements.

It is worthwhile to note that all models perform reasonably well for low to moderate discharge values (0-30 mm), but significant differences emerge at higher discharge events (>80 mm), which is crucial for flood forecasting. Although the proposed RCPIKLA model maintains better prediction accuracy for these high discharge events, there is room for improvement, which may be attributed to the limited number of high discharge events in the training



380

dataset. This systematic underestimation of peak flows represents a common challenge in hydrological modeling of Arctic rivers, where extreme discharge events are relatively rare but carry significant implications for water resource management and hazard mitigation. Future work could address this limitation through specialized sampling techniques or physics-informed constraints specifically designed to better capture high-magnitude discharge events.

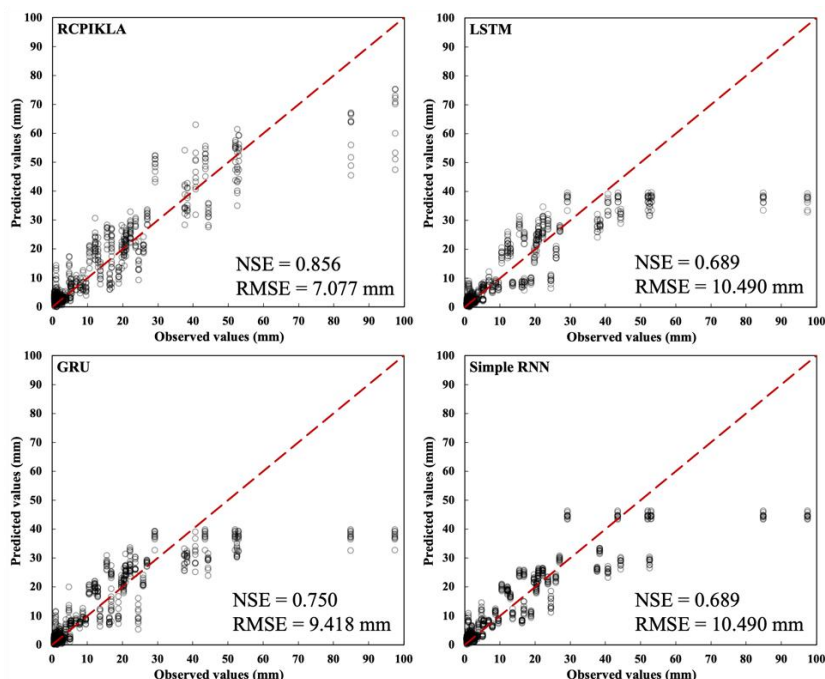


**Figure 7: The predicted and observed values of multiple models when the time step is 9 months, including RCPIKLA, LSTM, GRU and Simple RNN models.**

#### 4.3. On the role of the physics informed constrains and residual structure

To isolate and evaluate the contribution of the physics-informed constraints and the residual learning structure, ablation experiments, which have been adopted by many other studies (Zhi et al., 2023; Zhou, 2025), are conducted using three model variants in Fig. 8, including the complete RCPIKLA model (incorporating both physics-informed constraints and residual compensation), RCKLA-no physics-informed (retaining the residual structure but without physics constraints), and PIKLA-no residual (including physics-informed constraints but without residual compensation). The boxplot summarizes the NSE and RMSE values of three models for time steps ranging from 1 to 12 months in 10 independent runs. It reveals that the complete RCPIKLA model achieves the highest median NSE performance (approximately 0.83) with an interquartile range spanning from 0.81 to 0.84. The RCKLA model without physics-informed constraints shows a slightly lower median NSE (approximately 0.81) with greater variability in interquartile range from 0.79 to 0.83. The PIKLA model without residual compensation demonstrates the lowest median NSE performance (approximately 0.79) with an interquartile range from 0.78 to 0.81. The distribution of RMSE value is consistent with NSE values. These comparative results highlight two important

385

390



395 aspects of the model architecture: 1) The physics-informed constraints contribute to overall model robustness and  
performance stability. By incorporating physical principles of snowpack accumulation and melt processes through  
the specialized SnowpackLayer, the model better captures the underlying hydrological dynamics of the Arctic River  
system. The physics-informed loss function, which mathematically enforces the relationship between melted snow  
and discharge, helps maintain physical consistency in the predictions. 2) The residual compensation mechanism  
addresses model inadequacies by learning the systematic errors in the physics-based predictions. This is particularly  
400 valuable for handling complex nonlinear processes that are not fully captured by the simplified physical  
representations. The performance difference between PIKLA and RCPIKLA demonstrates that the residual structure  
successfully compensates for approximation errors in the physics-informed component. The synergistic integration  
of both components yields a new structure that balances data-driven flexibility with physical consistency. This  
hybrid approach is particularly advantageous in data-limited environments like Arctic Rivers, where the physics-  
405 informed constraints and the residual compensation help overcome model simplifications and data uncertainty.

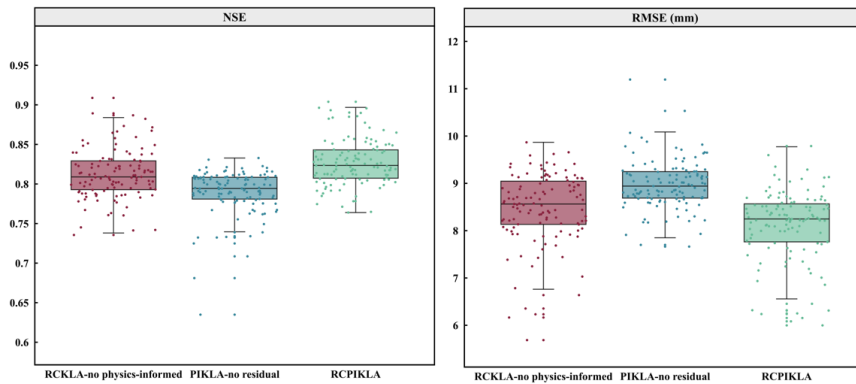


**Figure 8: The role of the residual structure and physics-informed constrains.**

#### 4.4. the role of seasonal variations and trigonometric encoding

Seasonality plays a significant role in Arctic hydrological systems (Häkkinen and Mellor, 1992), where discharge  
patterns are strongly influenced by annual cycles of temperature, snow accumulation, and melt. Accurately capturing  
such periodic behaviors is essential for robust long-term forecasting models. To address this, a trigonometric  
410 encoding (TE) of seasonal features is incorporated as input variables using sine and cosine transformations of the  
calendar month. Specifically, the timestamp is mapped to two features using the following equations:

$$\text{Month}_{\sin} = \sin\left(2\pi\frac{M}{12}\right); \text{Month}_{\cos} = \cos\left(2\pi\frac{M}{12}\right), \quad (23)$$

where  $M$  refers to the calendar month. These encodings aim at capturing cyclical temporal patterns without  
introducing artificial discontinuities between December and January. They are added to the input feature set of all  
415 models, which allows the proposed model to better associate temporal patterns with hydrometeorological signals.



As shown in Fig. 9, the box plot compares NSE and RMSE distributions for multiple model variants with and without trigonometric encoding (TE) of monthly seasonality. The results demonstrate that trigonometric encoding substantially improves performance across all model architectures. The proposed RCPIKLA model maintains the highest median NSE (approximately 0.83) with trigonometric encoding, while the removal of TE (denoted by "-no TE") leads to degraded performance (median NSE around 0.80) and wider value ranges. This pattern is consistent across all architectures, with GRU, LSTM, and Simple RNN models all exhibiting substantial performance degradation when seasonal encoding is removed. The widths of the box plots, representing interquartile ranges, also decrease substantially with TE, indicating greater consistency and reduced variability across model runs. Similar improvements are observed in GRU, LSTM, and Simple RNN models. In particular, the LSTM and Simple RNN models without trigonometric encoding show greater instability, with some runs achieving NSE values below 0.5, which shows severely compromised predictive capability. Regarding RMSE, the incorporation of TE effectively reduces median errors and decreases variability, particularly for RCPIKLA, where RMSE values exhibit the narrowest range. Outliers observed in models without trigonometric encoding suggest that omitting seasonal encodings can lead to occasional severe prediction errors, likely caused by the model's inability to account effectively for seasonal patterns.

Overall, the strong performance degradation observed when removing trigonometric encoding indicates the strong seasonality of Arctic River discharge. This seasonality can be characterized by processes including winter low flow due to frozen conditions, spring peak flow during snowmelt, and moderate summer flows influenced by rainfall and evapotranspiration. Without explicit encoding of this cyclical pattern, models struggle to establish accurate temporal context for the meteorological inputs, resulting in compromised predictive accuracy.

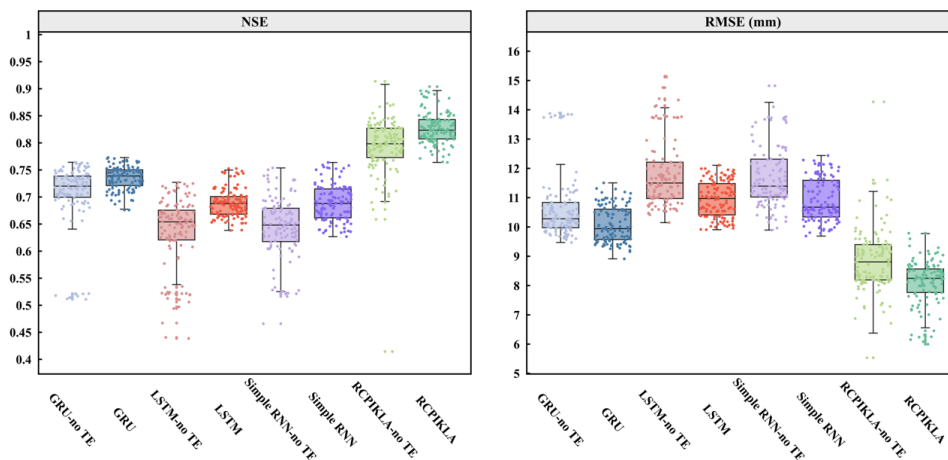


**Figure 9.** The comparison of models with and without trigonometric encoding for seasonal variations as inputs.

## 5. Conclusion





Arctic river systems play a critical role in global climate regulation, carbon cycling, and regional ecosystems, yet they remain challenging in hydrological modeling due to sparse data networks, the complex dynamics of permafrost-dominated landscapes, and nonlinear characteristics. In this study, a novel hybrid residual compensated deep learning model is proposed and designed specifically for Arctic River discharge forecasting. By integrating Kolmogorov-Arnold Networks (KAN), long short-term memory (LSTM) and the attention mechanism with seasonal encoding and physics-based constraints, the newly proposed approach aims at addressing the unique challenges of hydrological forecasting in permafrost-dominated regions, making it particularly valuable for modeling complex seasonal dynamics in Arctic River systems where snow accumulation and melt dominate discharge patterns. The KAN structure leverages the strengths of learnable activation functions and structured transformations to effectively extract nonlinear and intricate patterns from the input data. The newly proposed model is applied to the Kolyma River and compared with several baseline models, including LSTM, GRU, and simple RNN model for assessing the role and contribution of various components. Future applications could extend to other Arctic watersheds, snow-dominated river systems in mid-latitudes, and potentially other environmental domains. The results are summarized as follows:

- 1). The predictive performance of the newly proposed model and baseline models are plotted and evaluated across a range of time steps, from 1 to 12 months. As illustrated in Fig. 5, the newly proposed model consistently overperforms other baselines at all time steps and produces robust predictive performance. It obtains the highest NSE values ranging from 0.78 to 0.86 and the lowest RMSE values between 6.5 mm to 8.5 mm. The model performs the best at a time step of 9 months, suggesting that the permafrost covered Arctic River discharge exhibits a relatively long memory or delayed response to preceding hydrometeorological conditions.
- 2). The predictive performance across different discharge value ranges is further assessed to understand how well each model captures the full spectrum of hydrological variability. All models perform reasonably well for low to moderate discharge values (0-30 mm), but more obvious differences emerge at moderate and high discharge events. Although the proposed RCIKLA model maintains improved prediction accuracy, challenges remain in accurately predicting extreme high discharge events, with all models showing a tendency to underestimate peak flows. This limitation may be partially attributed to the relatively sparse representation of high discharge events in the dataset, which constrains the model's ability to generalize under extreme hydrological scenarios.
- 3). Both physics-informed constraints and residual compensation contribute distinctly to model performance. The physics-informed component, which incorporates snowpack accumulation and melt processes, provides the proposed model with basic domain knowledge that helps overcome data limitations in the permafrost-dominated Kolyma River basin. The residual compensation mechanism examines systematic errors in the physics-based predictions and helps capture complex nonlinear processes that are not fully represented.
- 4) By transforming month values into sine and cosine components that preserve the cyclical nature of seasonal patterns, the incorporation of trigonometric seasonal encoding can improve the predictive performance. This approach enhances prediction accuracy across all architectures, with improvements of 4-6% in performance metrics, highlighting the importance of representing the pronounced seasonal dynamics of Arctic rivers characterized by



frozen winter conditions, spring snowmelt peaks, and moderate summer flows. The trigonometric seasonal is particularly effective when combined with the RCPIKLA architecture.

#### 475 **Declaration of competing interest**

The author declares that he has no known competing financial interests or personal relationships that could have appeared to influence the work reported in this paper.

#### **Code/Data availability**

Data and code will be made available on request.

#### 480 **Author contribution**

RZ: Writing – original draft, Visualization, Validation, Resources, Methodology, Investigation, Formal analysis, Data curation, Conceptualization. SL: Writing – review & editing, Resources, Data curation, Investigation.

#### **Acknowledgement**

This research was supported by the U.S. National Science Foundation (Award# 2407963).

#### 485 **References**

- Alzubaidi, L., Bai, J., Al-Sabaawi, A., Santamaría, J., Albahri, A. S., Al-dabbagh, B. S. N., Fadhel, M. A., Manoufali, M., Zhang, J., Al-Timemy, A. H., Duan, Y., Abdullah, A., Farhan, L., Lu, Y., Gupta, A., Albu, F., Abbosh, A., and Gu, Y.: A survey on deep learning tools dealing with data scarcity: definitions, challenges, solutions, tips, and applications, *J Big Data*, 10, 46, <https://doi.org/10.1186/s40537-023-00727-2>, 2023.
- 490 An, L., Hao, Y., Yeh, T.-C. J., Liu, Y., Liu, W., and Zhang, B.: Simulation of karst spring discharge using a combination of time–frequency analysis methods and long short-term memory neural networks, *Journal of Hydrology*, 589, 125320, <https://doi.org/10.1016/j.jhydrol.2020.125320>, 2020.
- Andersson, T. R., Hosking, J. S., Pérez-Ortiz, M., Paige, B., Elliott, A., Russell, C., Law, S., Jones, D. C., Wilkinson, J., Phillips, T., Byrne, J., Tietsche, S., Sarojini, B. B., Blanchard-Wrigglesworth, E., Aksenov, Y., Downie, R., and  
495 Shuckburgh, E.: Seasonal Arctic sea ice forecasting with probabilistic deep learning, *Nat Commun*, 12, 5124, <https://doi.org/10.1038/s41467-021-25257-4>, 2021.
- Bakhshi Ostadkalayeh, F., Moradi, S., Asadi, A., Moghaddam Nia, A., and Taheri, S.: Performance Improvement of LSTM-based Deep Learning Model for Streamflow Forecasting Using Kalman Filtering, *Water Resour Manage*, 37, 3111–3127, <https://doi.org/10.1007/s11269-023-03492-2>, 2023.
- 500 Basu, B., Morrissey, P., and Gill, L. W.: Application of Nonlinear Time Series and Machine Learning Algorithms for Forecasting Groundwater Flooding in a Lowland Karst Area, *Water Resources Research*, 58, e2021WR029576, <https://doi.org/10.1029/2021WR029576>, 2022.



- 505 Bring, A., Fedorova, I., Dibike, Y., Hinzman, L., Mård, J., Mernild, S. H., Prowse, T., Semenova, O., Stuefer, S. L., and Woo, M. -K.: Arctic terrestrial hydrology: A synthesis of processes, regional effects, and research challenges, *JGR Biogeosciences*, 121, 621–649, <https://doi.org/10.1002/2015JG003131>, 2016.
- D. N. Moriasi, J. G. Arnold, M. W. Van Liew, R. L. Bingner, R. D. Harmel, and T. L. Veith: Model Evaluation Guidelines for Systematic Quantification of Accuracy in Watershed Simulations, *Transactions of the ASABE*, 50, 885–900, <https://doi.org/10.13031/2013.23153>, 2007.
- 510 DeWalle, D. R. and Rango, A.: *Principles of Snow Hydrology*, 1st ed., Cambridge University Press, <https://doi.org/10.1017/CBO9780511535673>, 2008.
- Ernakovich, J. G., Hopping, K. A., Berdanier, A. B., Simpson, R. T., Kachergis, E. J., Steltzer, H., and Wallenstein, M. D.: Predicted responses of arctic and alpine ecosystems to altered seasonality under climate change, *Global Change Biology*, 20, 3256–3269, <https://doi.org/10.1111/gcb.12568>, 2014.
- 515 Feng, D., Gleason, C. J., Lin, P., Yang, X., Pan, M., and Ishitsuka, Y.: Recent changes to Arctic river discharge, *Nat Commun*, 12, 6917, <https://doi.org/10.1038/s41467-021-27228-1>, 2021.
- Gao, S., Huang, Y., Zhang, S., Han, J., Wang, G., Zhang, M., and Lin, Q.: Short-term runoff prediction with GRU and LSTM networks without requiring time step optimization during sample generation, *Journal of Hydrology*, 589, 125188, <https://doi.org/10.1016/j.jhydrol.2020.125188>, 2020.
- 520 Gelfan, A., Gustafsson, D., Motovilov, Y., Arheimer, B., Kalugin, A., Krylenko, I., and Lavrenov, A.: Climate change impact on the water regime of two great Arctic rivers: modeling and uncertainty issues, *Climatic Change*, 141, 499–515, <https://doi.org/10.1007/s10584-016-1710-5>, 2017.
- Granata, F., Zhu, S., and Di Nunno, F.: Advanced streamflow forecasting for Central European Rivers: The Cutting-Edge Kolmogorov-Arnold networks compared to Transformers, *Journal of Hydrology*, 645, 132175, <https://doi.org/10.1016/j.jhydrol.2024.132175>, 2024.
- 525 Häkkinen, S. and Mellor, G. L.: Modeling the seasonal variability of a coupled Arctic ice-ocean system, *J. Geophys. Res.*, 97, 20285–20304, <https://doi.org/10.1029/92JC02037>, 1992.
- Harpold, A. A., Kaplan, M. L., Klos, P. Z., Link, T., McNamara, J. P., Rajagopal, S., Schumer, R., and Steele, C. M.: Rain or snow: hydrologic processes, observations, prediction, and research needs, *Hydrol. Earth Syst. Sci.*, 21, 1–22, <https://doi.org/10.5194/hess-21-1-2017>, 2017.
- 530 Harris, I., Osborn, T. J., Jones, P., and Lister, D.: Version 4 of the CRU TS monthly high-resolution gridded multivariate climate dataset, *Sci Data*, 7, 109, <https://doi.org/10.1038/s41597-020-0453-3>, 2020.
- Hochreiter, S. and Schmidhuber, J.: Long Short-Term Memory, *Neural Computation*, 9, 1735–1780, <https://doi.org/10.1162/neco.1997.9.8.1735>, 1997.
- 535 Hock, R.: Temperature index melt modelling in mountain areas, *Journal of Hydrology*, 282, 104–115, [https://doi.org/10.1016/S0022-1694\(03\)00257-9](https://doi.org/10.1016/S0022-1694(03)00257-9), 2003.
- Holmes, R. M., McClelland, J. W., Peterson, B. J., Tank, S. E., Bulygina, E., Eglinton, T. I., Gordeev, V. V., Gurtovaya, T. Y., Raymond, P. A., Repeta, D. J., Staples, R., Striegl, R. G., Zhulidov, A. V., and Zimov, S. A.: Seasonal and Annual Fluxes of Nutrients and Organic Matter from Large Rivers to the Arctic Ocean and Surrounding Seas, *Estuaries and Coasts*, 35, 369–382, <https://doi.org/10.1007/s12237-011-9386-6>, 2012.
- 540 Jin, A., Wang, Q., Zhan, H., and Zhou, R.: Comparative Performance Assessment of Physical-Based and Data-Driven Machine-Learning Models for Simulating Streamflow: A Case Study in Three Catchments across the US, *J. Hydrol. Eng.*, 29, 05024004, <https://doi.org/10.1061/JHYEFF.HEENG-6118>, 2024a.



- 545 Jin, A., Wang, Q., Zhou, R., Shi, W., and Qiao, X.: Hybrid Multivariate Machine Learning Models for Streamflow Forecasting: A Two-Stage Decomposition–Reconstruction Framework, *J. Hydrol. Eng.*, 29, 04024026, <https://doi.org/10.1061/JHYEFF.HEENG-6254>, 2024b.
- Karniadakis, G. E., Kevrekidis, I. G., Lu, L., Perdikaris, P., Wang, S., and Yang, L.: Physics-informed machine learning, *Nat Rev Phys*, 3, 422–440, <https://doi.org/10.1038/s42254-021-00314-5>, 2021.
- 550 Kratzert, F., Klotz, D., Brenner, C., Schulz, K., and Herrnegger, M.: Rainfall–runoff modelling using Long Short-Term Memory (LSTM) networks, *Hydrol. Earth Syst. Sci.*, 22, 6005–6022, <https://doi.org/10.5194/hess-22-6005-2018>, 2018.
- Krogh, S. A., Pomeroy, J. W., and Marsh, P.: Diagnosis of the hydrology of a small Arctic basin at the tundra-taiga transition using a physically based hydrological model, *Journal of Hydrology*, 550, 685–703, <https://doi.org/10.1016/j.jhydrol.2017.05.042>, 2017.
- 555 Kůrková, V.: Kolmogorov’s theorem and multilayer neural networks, *Neural Networks*, 5, 501–506, [https://doi.org/10.1016/0893-6080\(92\)90012-8](https://doi.org/10.1016/0893-6080(92)90012-8), 1992.
- Liu, Z., Wang, Y., Vaidya, S., Ruehle, F., Halverson, J., Soljačić, M., Hou, T. Y., and Tegmark, M.: KAN: Kolmogorov-Arnold Networks, <https://doi.org/10.48550/ARXIV.2404.19756>, 2024.
- 560 McClelland, J. W., Holmes, R. M., Peterson, B. J., and Stieglitz, M.: Increasing river discharge in the Eurasian Arctic: Consideration of dams, permafrost thaw, and fires as potential agents of change, *J. Geophys. Res.*, 109, 2004JD004583, <https://doi.org/10.1029/2004JD004583>, 2004.
- Peterson, B. J., Holmes, R. M., McClelland, J. W., Vörösmarty, C. J., Lammers, R. B., Shiklomanov, A. I., Shiklomanov, I. A., and Rahmstorf, S.: Increasing River Discharge to the Arctic Ocean, *Science*, 298, 2171–2173, <https://doi.org/10.1126/science.1077445>, 2002.
- 565 Prowse, T., Alfredsen, K., Beltaos, S., Bonsal, B. R., Bowden, W. B., Duguay, C. R., Korhola, A., McNamara, J., Vincent, W. F., Vuglinsky, V., Walter Anthony, K. M., and Weyhenmeyer, G. A.: Effects of Changes in Arctic Lake and River Ice, *AMBIO*, 40, 63–74, <https://doi.org/10.1007/s13280-011-0217-6>, 2011.
- Rawlins, M. A. and Karmalkar, A. V.: Regime shifts in Arctic terrestrial hydrology manifested from impacts of climate warming, *The Cryosphere*, 18, 1033–1052, <https://doi.org/10.5194/tc-18-1033-2024>, 2024.
- 570 Schneider, U., Hänsel, S., Finger, P., Rustemeier, E., and Ziese, M.: GPCC Full Data Monthly Version 2022 at 2.5°: Monthly Land-Surface Precipitation from Rain-Gauges built on GTS-based and Historic Data: Globally Gridded Monthly Totals (2022), [https://doi.org/10.5676/DWD\\_GPCC/FD\\_M\\_V2022\\_250](https://doi.org/10.5676/DWD_GPCC/FD_M_V2022_250), 2022.
- Sergeev, A., Baglaeva, E., and Subbotina, I.: Hybrid model combining LSTM with discrete wavelet transformation to predict surface methane concentration in the Arctic Island Belyy, *Atmospheric Environment*, 317, 120210, <https://doi.org/10.1016/j.atmosenv.2023.120210>, 2024.
- 575 Singh, A., Kalke, H., Loewen, M., and Ray, N.: River Ice Segmentation With Deep Learning, *IEEE Trans. Geosci. Remote Sensing*, 58, 7570–7579, <https://doi.org/10.1109/TGRS.2020.2981082>, 2020.
- Spencer, R. G. M., Mann, P. J., Dittmar, T., Eglinton, T. I., McIntyre, C., Holmes, R. M., Zimov, N., and Stubbins, A.: Detecting the signature of permafrost thaw in Arctic rivers, *Geophysical Research Letters*, 42, 2830–2835, <https://doi.org/10.1002/2015GL063498>, 2015.
- 580 Tank, S. E., McClelland, J. W., Spencer, R. G. M., Shiklomanov, A. I., Suslova, A., Moatar, F., Amon, R. M. W., Cooper, L. W., Elias, G., Gordeev, V. V., Guay, C., Gurtovaya, T. Yu., Kosmenko, L. S., Mutter, E. A., Peterson, B. J., Peucker-Ehrenbrink, B., Raymond, P. A., Schuster, P. F., Scott, L., Staples, R., Striegl, R. G., Tretiakov, M.,



- Zhulidov, A. V., Zimov, N., Zimov, S., and Holmes, R. M.: Recent trends in the chemistry of major northern rivers signal widespread Arctic change, *Nat. Geosci.*, 16, 789–796, <https://doi.org/10.1038/s41561-023-01247-7>, 2023a.
- 585 Tank, S. E., McClelland, J. W., Spencer, R. G. M., Shiklomanov, A. I., Suslova, A., Moatar, F., Amon, R. M. W., Cooper, L. W., Elias, G., Gordeev, V. V., Guay, C., Gurtovaya, T. Yu., Kosmenko, L. S., Mutter, E. A., Peterson, B. J., Peucker-Ehrenbrink, B., Raymond, P. A., Schuster, P. F., Scott, L., Staples, R., Striegl, R. G., Tretiakov, M., Zhulidov, A. V., Zimov, N., Zimov, S., and Holmes, R. M.: Recent trends in the chemistry of major northern rivers signal widespread Arctic change, *Nat. Geosci.*, 16, 789–796, <https://doi.org/10.1038/s41561-023-01247-7>, 2023b.
- 590 Vaswani, A., Shazeer, N., Parmar, N., Uszkoreit, J., Jones, L., Gomez, A. N., Kaiser, Ł., and Polosukhin, I.: Attention is All you Need, in: *Advances in Neural Information Processing Systems*, 2017.
- Vonk, J. E., Fritz, M., Speetjens, N. J., Babin, M., Bartsch, A., Basso, L. S., Bröder, L., Göckede, M., Gustafsson, Ö., Hugelius, G., Irrgang, A. M., Juhls, B., Kuhn, M. A., Lantuit, H., Manizza, M., Martens, J., O'Regan, M., Suslova, A., Tank, S. E., Terhaar, J., and Zolkos, S.: The land–ocean Arctic carbon cycle, *Nat Rev Earth Environ*, 6, 86–105, <https://doi.org/10.1038/s43017-024-00627-w>, 2025.
- 595 Walvoord, M. A. and Kurylyk, B. L.: Hydrologic Impacts of Thawing Permafrost—A Review, *Vadose Zone Journal*, 15, 1–20, <https://doi.org/10.2136/vzj2016.01.0010>, 2016.
- Wang, P., Huang, Q., Pozdniakov, S. P., Liu, S., Ma, N., Wang, T., Zhang, Y., Yu, J., Xie, J., Fu, G., Frolova, N. L., and Liu, C.: Potential role of permafrost thaw on increasing Siberian river discharge, *Environ. Res. Lett.*, 16, 034046, <https://doi.org/10.1088/1748-9326/abe326>, 2021.
- 600 Xie, K., Liu, P., Zhang, J., Han, D., Wang, G., and Shen, C.: Physics-guided deep learning for rainfall-runoff modeling by considering extreme events and monotonic relationships, *Journal of Hydrology*, 603, 127043, <https://doi.org/10.1016/j.jhydrol.2021.127043>, 2021.
- Yang, S., Yang, D., Chen, J., Santisirisomboon, J., Lu, W., and Zhao, B.: A physical process and machine learning combined hydrological model for daily streamflow simulations of large watersheds with limited observation data, *Journal of Hydrology*, 590, 125206, <https://doi.org/10.1016/j.jhydrol.2020.125206>, 2020.
- 605 Zhang, S., Gan, T. Y., Bush, A. B. G., and Zhang, G.: Evaluation of the impact of climate change on the streamflow of major pan-Arctic river basins through machine learning models, *Journal of Hydrology*, 619, 129295, <https://doi.org/10.1016/j.jhydrol.2023.129295>, 2023.
- 610 Zhi, W., Ouyang, W., Shen, C., and Li, L.: Temperature outweighs light and flow as the predominant driver of dissolved oxygen in US rivers, *Nat Water*, 1, 249–260, <https://doi.org/10.1038/s44221-023-00038-z>, 2023.
- Zhong, L., Lei, H., and Yang, J.: Development of a Distributed Physics-Informed Deep Learning Hydrological Model for Data-Scarce Regions, *Water Resources Research*, 60, e2023WR036333, <https://doi.org/10.1029/2023WR036333>, 2024.
- 615 Zhou, R.: Multi-scale dynamic spatiotemporal graph attention network for forecasting karst spring discharge, *Journal of Hydrology*, 133289, <https://doi.org/10.1016/j.jhydrol.2025.133289>, 2025.
- Zhou, R. and Zhang, Y.: On the role of the architecture for spring discharge prediction with deep learning approaches, *Hydrol. Process.*, 36, <https://doi.org/10.1002/hyp.14737>, 2022a.
- 620 Zhou, R. and Zhang, Y.: Reconstruction of missing spring discharge by using deep learning models with ensemble empirical mode decomposition of precipitation, *Environ. Sci. Pollut. Res.*, <https://doi.org/10.1007/s11356-022-21597-w>, 2022b.
- Zhou, R. and Zhang, Y.: Linear and nonlinear ensemble deep learning models for karst spring discharge forecasting, *J. Hydrol.*, 627, 130394, <https://doi.org/10.1016/j.jhydrol.2023.130394>, 2023a.



- 625 Zhou, R. and Zhang, Y.: Predicting and explaining karst spring dissolved oxygen using interpretable deep learning approach, *Hydrol. Process.*, 37, e14948, <https://doi.org/10.1002/hyp.14948>, 2023b.
- Zhou, R., Zhang, Y., Wang, Q., Jin, A., and Shi, W.: A hybrid self-adaptive DWT-WaveNet-LSTM deep learning architecture for karst spring forecasting, *J. Hydrol.*, 634, 131128, <https://doi.org/10.1016/j.jhydrol.2024.131128>, 2024a.
- 630 Zhou, R., Wang, Q., Jin, A., Shi, W., and Liu, S.: Interpretable multi-step hybrid deep learning model for karst spring discharge prediction: Integrating temporal fusion transformers with ensemble empirical mode decomposition, *J. Hydrol.*, 132235, <https://doi.org/10.1016/j.jhydrol.2024.132235>, 2024b.